Ferreira et al. *Journal of Mathematics in Industry* (2024) 14:1
https://doi.org/10.1186/s13362-023-00139-0

Journal of Mathematics in Industry
a SpringerOpen Journal

RESEARCH **Open Access**

Respiratory particles: from analytical estimates to disease transmission

J.A. Ferreira[1], Paula de Oliveira[1*] and P.M. da Silva[1,2]

*Correspondence: poliveir@mat.uc.pt
[1]Centre of Mathematics of the University of Coimbra, University of Coimbra, FCTUC, 3030 Coimbra, Portugal
Full list of author information is available at the end of the article

Abstract

Respiratory particles containing infectious pathogens are responsible for a large number of diseases. To define health politics and save lives, it is important to study their transmission mechanisms, namely the path of particles once expelled. This path depends on several driving factors as intrinsic properties of particles, environmental aspects and morphology of the scenario. Following physical arguments and taking into account the results of experimental works, we consider a mathematical drift model for the mixture composed by two phases: air and particles. The relative motion between the two phases is described by a kinematic constitutive relation. We prove the stability of the model for fixed times and establish an a priori estimate for the total number of infectious particles. The upper bound of this estimate exhibits sound physical dependencies on the driving factors, in agreement with the experimental literature and mounting epidemiological evidences. Namely, we establish that the amount of particles expelled and their emission rate can explain why some people are superspreaders. Several numerical simulations illustrate the theoretical results.

Keywords: Respiratory particles; Evaporation; Settling; Partial differential equations; Drift model; Estimates; Numerical simulation

1 Introduction

Biological motivation A large number of diseases are spread by respiratory particles, due to the possible presence of infectious pathogens, virus, bacteria or fungi, in their nuclei. These particles can be exhaled by all kind of respiratory events from breathing and talking, to the most violent ones as coughing and sneezing. In the last decades, the problem of air quality and airborne diseases transmission - as for example influenza, tuberculosis, measles and Covid-19 - drew the attention of a very large number of researchers working in different applied and experimental areas [5–28].

During Covid-19 pandemy applied researchers have produced a large number of works [4–18] on airborne disease transmission and this had an important role in health politics and into saving lives. Our objective in this paper is to establish analytically experimental results of the above mentioned works and conclusions from epidemiological findings. With this goal we propose a model based on a system of ordinary differential equations, ODEs, for the particle velocity and a system of partial differential equations, PDEs, for the particle concentration. The steady state of the system of ODEs gives the settling velocity,

that is used as the relative velocity of particles with respect to air flow. The PDEs system is composed by a Navier-Stokes equation and a convection-diffusion-reaction equation. The convection field in this last equation is represented by the sum of the settling velocity with the air flow velocity given by the numerical solution of Navier-Stokes equation. An expression for the settling velocity can be deduced analitically from the steady solution of the system of ODEs.

To establish the model we must understand what happens to respiratory droplets once exhaled. After exhalation, the space-time evolution of respiratory droplets depends on several driving factors (Fig. 1): properties of droplets, environmental factors and morphology of the scenario. Regarding these driving factors, we find several references in the literature as for example:

(i) Properties of droplets: amount, size, emission rate and viral load of exhaled particles ([3, 4, 27]);
(ii) Environmental factors: relative humidity (RH), temperature and ventilation ([4, 20]);
(iii) Morphology of the scenario: obstacles and materials ([1, 13, 28]).

In what follows we present some comments on the influence of these factors. The droplet radii, measured in different experimental works (for example [27]), are reported to be in the range 0.5 - 1000 micrometers (μm). However around 95% have radii in the interval $[1, 60]$. This size distribution appears largely independent of the type of respiratory event. On the contrary, the number of exhaled droplets depends mainly on the type of respiratory event: a few thousand for a cough, up to a million for a sneeze. The fate of respiratory droplets, emitted by an infected person during a respiratory event, is different for "large" and "small" particles. The definition of "small" and "large" is based on experimental results and the radius size cut-off has variations from study to study. Currently the World Health Organization guidelines define this cut-off at 5 μm. "Large" particles fall on available deposition surfaces, within a short time, and can produce contamination by direct contact; "small" particles stay suspended in the air for longer periods and can be inhaled by other people in the same space ([3]). This type of contamination is called airborne transmission. The two environmental properties that influence the fate of respiratory particles, once expelled from the respiratory tract, are humidity and temperature. Regarding humidity the concept used in the present paper is relative humidity (RH), which quantifies the amount of moisture the air can hold. RH depends on absolute humidity and temperature. As the temperature increases, the air can hold more moisture and the relative humidity increases. Consequently, when the concept of RH is used the influence of temperature on evaporation is also taken into account. In fact RH influences the fate of respiratory particles for two different reasons. Firstly, low RH accelerates evaporation, reduces the radius of particles and consequently their weight, what makes them stay suspended in the air longer. Secondly, RH governs the survival of pathogens inside the droplets. The relation between RH and virus inactivation rate is a complex one and it is represented by an U-shaped function, for a large number of virus ([1]). Regarding the direct role of temperature in the virus viability, there are different conclusions in the literature. As mentioned in [4] and the references therein, "there is little scientific evidence to suggest that lower winter temperatures are important direct drivers of wintertime seasonality of respiratory infections. In particular, in indoor environments, where people spend 90% of their time and where most infections occur, temperature does not vary much since buildings are heated as it gets cooler outdoors". It was following these arguments that we chose not to consider the

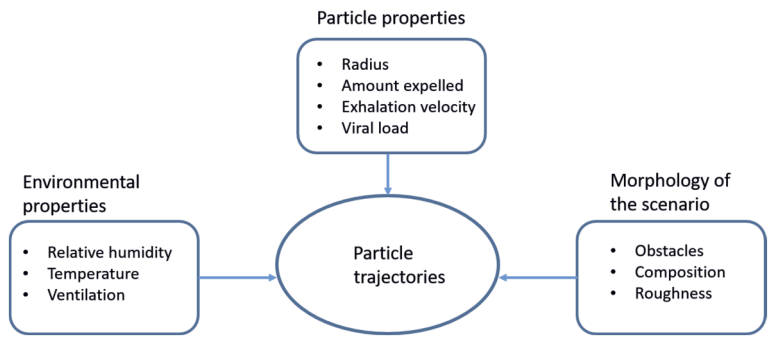

Figure 1 The space-time evolution of respiratory particles depends on several driving factors

direct effect of temperature on the viability of the virus. However, future developments of the mathematical model should include the influence of temperature on the inactivation rate of virus ([29]).

As what concerns ventilation, different systems can be considered from passive to forced ventilation. With reference to the morphology of the scenario, several aspects can be examined as deposition on the vertical walls, on the floor, or on the furniture. To keep the model as simple as possible, while taking into account the main phenomena involved, we will use a simplified description of deposition based on a global deposition rate ([1]). Figure 1 shows a diagram of the main factors governing the trajectory of respiratory particles.

Which is the interplay between these factors? Particles are expelled from the respiratory system, dispersed in the air and the water vapour flow. Once expelled, particles enter unsaturated air, travel under the action of convection, diffusion and gravity. They start to evaporate and their radii decrease: the largest particles are deposed on available surfaces and the smallest particles stay suspended in the air. The amount by which a particle radius decreases depends on its initial radius, the fraction of non volatile matter in the droplet nuclei-including pathogens, sugars, proteins, lipids - and on the relative humidity in the domain ([4]). As the radius shrinks, the droplet loses water vapour, and its density increases because nuclei are denser than the water vapour where they are entrapped: the higher RH, the lower is the evaporation rate (Fig. 2).

Mathematical models in the literature The flow of respiratory droplets suspended in the air can be considered a two-phase disperse flow. To model disperse flows, two main approaches can be found in the literature: trajectory models and two-fluid models. In the trajectory models, the motion of the disperse phase - the particles - is governed by Newton's second law, taking into account gravity, buoyancy, drag force and the force responsible for the momentum destruction of vapour due to evaporation. The models based on this physical description, are described by two coupled ordinary differential equations (ODEs) for each particle. One of the equations is used to compute the velocity and the other to define the position occupied by the particle ([3, 6, 23–25]). The ODEs systems for the velocity u_p and the position s of a particle, with a certain initial radius, are of the form

$$\begin{cases} \frac{d(m_p u_p)}{dt} = F_g + F_b + F_d + F_s, \\ \frac{ds}{dt} = u_p, \end{cases} \tag{1}$$

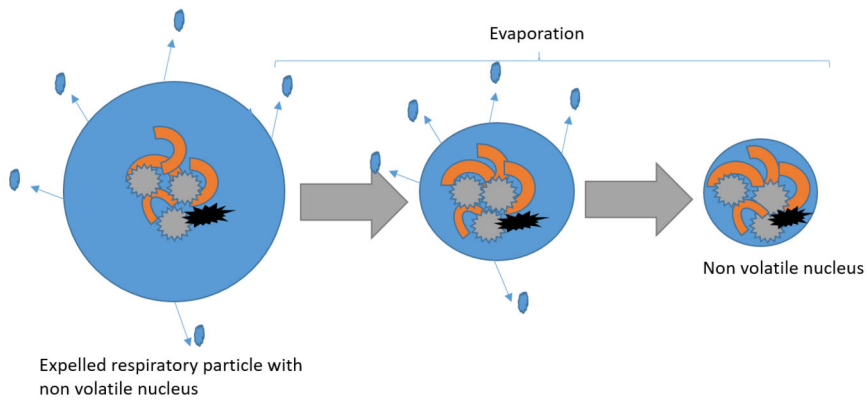

Figure 2 Evaporation process in particles with non volatile nuclei. The higher is the relative humidity, the lower is the evaporation rate

where m_p represents the time-dependent mass of the particle, F_g stands for the gravity force, F_b represents the buoyancy, F_d the drag force and F_s represents the force responsible for the momentum destruction of vapour due to evaporation. In system (1) and the following, t represents the time measured in seconds. System (1) is closed with initial conditions for u_p and s. Regarding trajectory models, we mention without being exhaustive, a number of formulations based on system (1), found in the literature and progressively more realistic:

(i) The simplest formulation considers that the respiratory droplets move in a static air following a ballistic trajectory after leaving the exhaled flow ([6]). The path of large droplets is dominated by gravity while the trajectories of small droplets can remain longer suspended in the air, leading to a greater dissemination. This means that large droplets tend to fall in seconds, depositing on surfaces and small droplets can travel for a longer period, being eventually inhaled by someone else. The conclusions are qualitatively in agreement with experimental results.

(ii) The experimental set up in [3] and [25] suggests that the path of particles is influenced by the respiratory flow. Following this rationale, system (1) was modified by including in the drag force F_d a velocity for the expelled air: an empiric velocity ([25]), or a velocity described by Navier-Stokes equations ([21, 23]).

(iii) In a third type of trajectory models found in the literature, the fluid flow behavior of droplets is modelled using two different systems, one for large and the other for small droplets. For large droplets it is used Newton's Law, where the velocity of the expelled air is computed by Navier-Stokes equations as in (ii); however the path of single small particles is omitted and is described by the fluid flow governed by Navier-Stokes and mass transfer equations ([16, 21]).

In the second approach for dispersed flows called two fluid model, the discrete nature of particles is overlooked and the dispersed phase is treated as a continuous phase. In this approach, conservation equations are developed for the two flows, which presents many difficulties related to the interactions between the two phases ([12]). A simplified version of two fluid model is the drift flux model where the mixture is considered as a whole, rather than composed by two separate phases. The formulation involves two mass conservation equations, one for each phase, and one momentum equation for the mixture.

The mass conservation of the dispersed phase is modelled by using a drift equation, that includes the relative velocity between the phases. Approximations of this relative velocity,can be computed iteratively from the steady state solution of the ODEs system. The no need of interface terms between the phases, the well-posedness, and the reduced number of transport equations represent some of the main advantages of the drift flux model. A theoretical framework in which these two formulations - two fluid model and drift flux model - are unified has been presented in [8]. Drift flux models have been used to simulate the quality of air ([5, 28, 31]). In some of these works the numerical results have been validated by experimental results ([5, 28]).

The present contribution In the present paper, we are interested in indoor propagation of respiratory particles, possibly leading to airborne contamination. We follow the general principles of drift flux models, as detailed in Sect. 2.3: one equation for the momentum of mixture, two equations for mass conservation, taking into account the drift velocity of particles relatively to the fluid. The evaporation of particles is considered in the present model which implies that their radii and densities are time depending. Our focus is the study of mathematical aspects related to theoretical estimates. Namely, we want to analyse if, from these theoretical estimates, it is possible to conclude the type of dependence on the driving factors, established by experimentalists.

The topic of airborne contamination has always attracted the attention of a very large number of researchers from applied areas, contributing with laboratorial results or numerical simulations. We believe that our approach represents an original contribution as it shows that the mathematical analysis of a priori estimates exhibits sound physical properties, leading to results in line with experimental work or mounting epidemiological evidence. We mention specifically the role of superspreaders as main drivers of respiratory infections outbreaks ([14]); the influence of RH in seasonality infections ([4]); the recommendations of health authorities concerning social distance and ventilation of indoor spaces.

The paper is structured as follows. In Sect. 2 we establish the equations, following the principles of drift flux models for disperse flows. The stability of the mathematical model is then deduced in Sect. 3. An a priori estimate of the total number of particles highlights the relative weight of the different driving factors, and supports a number of health guidelines adopted to block disease spread. The estimates are numerically illustrated and compared with results in the experimental literature. In Sect. 4 several numerical experiments are presented. In Sect. 5 some conclusions are addressed.

2 Mathematical model

In this section we present a mathematical model that describes the evolution of the number density of respiratory droplets exhaled indoors, during a violent respiratory event - coughing or sneezing. It is assumed that particles are laden with virus and that evaporation takes place after expulsion. Moreover we assume that ventilation is guaranteed by a passive system.

We consider a drift flux model ([5, 8, 10, 12]) where the mixture composed by two phases - air and particles - is viewed as a whole and the relative motion between the two phases is described by a kinematic constitutive relation.

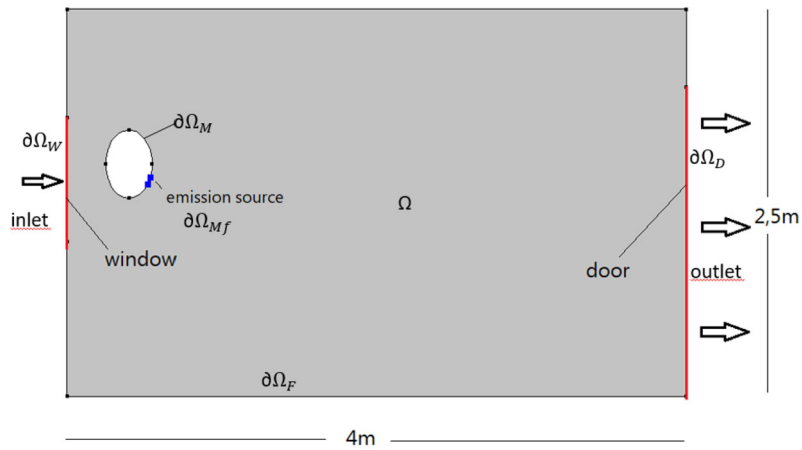

Figure 3 A vertical slice of the domain. In the numerical illustrations the domain is two-dimensional with 4 m wide and 2.5 m high

2.1 Convection-diffusion-reaction equation for the dispersed phase

Let $\Omega \subset \mathbb{R}^n$, $n = 2, 3$, represents the physical domain where the evolution of respiratory droplets is studied. Let the boundary $\partial\Omega$ be decomposed in

$$\partial\Omega = \partial\Omega_W \cup \partial\Omega_D \cup \partial\Omega_F \cup \partial\Omega_{w_a} \cup \partial\Omega_{M_f} \cup \partial\Omega_{M_b}$$

as represented in Fig. 3. The boundaries $\partial\Omega_W$ and $\partial\Omega_D$ represent two openings of a passive ventilation system, a window and a door respectively; $\partial\Omega_F$ stands for the floor of the room. Ω_M stands for the location of the emission source and its boundary satisfies $\partial\Omega_M = \partial\Omega_{M_f} \cup \partial\Omega_{M_b}$, where $\partial\Omega_{M_f}$ represents the entry of the respiratory flow in Ω. Ω_M stands for the head of an issuer that stands in the domain and is represented by an ellipse. Finally $\partial\Omega_{w_a}$ represents the remaining boundaries. We note that the theoretical estimates in Sect. 3 hold for $n = 2, 3$.

The respiratory particles are assumed spherical with radius $R(t)$ and density $\rho_p(t)$. We suppose that evaporation takes place as the particles are expelled, which explains that radius and density are time dependent. We also assume that particles, while evaporating, keep their spherical shape. To guarantee that the particles can be considered in the continuum regime and that the usual equations of continuum mechanics can be applied, we assume that the Knudsen number, $k_n = \frac{\lambda}{R(t)} \ll 1$, where λ is the mean free path of air molecules. The inequality is satisfied for an initial radius $R_0 \gg 0.0651\,\mu m$ ([9]) and consequently the continuum regime can be used for particles with radii exceeding this value.

Let $C(x, t)$ stand for the number of particles per unit volume, designated by the number density of respiratory particles. We assume all the particles have infectious nuclei and an initial radius R_0. The total mass of particles, with infectious nuclei and with initial radius R_0, in A is given by

$$M(t) = \int_A m_p(t)\, C(x, t)\, dx, \tag{2}$$

where $A \subset \Omega$ represents an arbitrary reference domain and $m_p(t)$ represents the mass of a particle, that is defined by $m_p(t) = \frac{4}{3}\pi R^3(t)\rho_p(t)$. We assume that the density $\rho_p(t)$, the mass

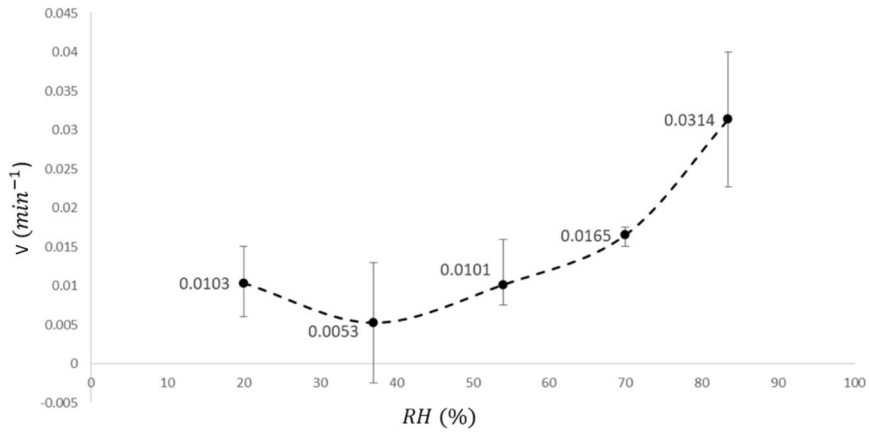

Figure 4 Inactivation rate of SARS-CoV-2 as a function of RH under a temperature of $T = 20°C$ ([1])

$m_p(t)$ and the radius $R(t)$ are the same for all the particles at time t, changing only with time. We postpone the theoretical measurement of ρ_p to Sect. 2.2. The variation of $M(t)$ in A is due to the flux J that crosses its boundary ∂A, to the deposition, to the inactivation of pathogens and the loss of mass by evaporation. J is a particle flux associated to $C(x,t)$, that will be defined in Sect. 2.4. To take into account these phenomena we write

$$\begin{aligned}\frac{dM}{dt}(t) = &-\int_{\partial A} m_p(t)J(s,t)\cdot\eta\, ds - \int_A m_p(t)KC(x,t)\, dx\\ &-\int_A m_p(t)VC(x,t)\, dx - \int_A m_p(t)L(t)C(x,t)\, dx.\end{aligned} \tag{3}$$

The sinks of the model, K and V, stand for the deposition of particles and the inactivation rate of the pathogens, respectively. The deposition of particles K, defined later in this section, is represented by a global deposition rate depending on a certain number of parameters ([1]). Regarding the inactivation rate V, it depends on several parameters, as defined in Sect. 4. It is represented, for most virus, by an U-shaped function. In Fig. 4 it is exhibited a plot of the inactivation rate of SARS-CoV-2 as a function of RH. The plot results from experimental works under a temperature of $T = 20°C$ ([1]). In equation (3), η stands for the exterior unit normal to ∂A.

As already mentioned in Sect. 1, we assume that, indoors, the inactivation rate depends essentially on relative humidity ([1, 4, 20]). The study presented in Sect. 3, follows the same lines that it would follow in the case the inativation rate V also depended directly on temperature. In the last term of the second member of equation (3), that quantifies mass loss by evaporation, the time function $L = L(t)$ stands for the rate of evaporation.

From equation (2) and equation (3) we have

$$m_p\frac{\partial C}{\partial t} + \frac{dm_p}{dt}C = -m_p\nabla\cdot J - m_pKC - m_pV(RH)C - m_pLC, \tag{4}$$

where we omitted the time and space variables. We recall that C and J are space-time functions, m_p and L are time functions, K and V are constants depending on several parameters.

Let us assume that the droplets don't evaporate completely up to the time T_e, that is $m_p(t) \neq 0, \forall t \in [0, T_e]$ where $[0, T_e]$ represents the time interval we are interested in. This is justified in the next paragraph.

As $\frac{dm_p}{dt} < 0$, the rate of evaporation L can be defined by

$$L = -\frac{\frac{dm_p}{dt}}{m_p} \tag{5}$$

and we deduce from equations (4) and (5) that the number density of particles with infectious nuclei satisfies

$$\frac{\partial C}{\partial t} = -\nabla \cdot J - (K + V)C \quad \text{in } \Omega \times (0, T_e]. \tag{6}$$

The emission of virus laden particles is represented by a boundary condition active on $\partial\Omega_{M_f}$ as the respiratory event lasts (Fig. 3).

2.2 Particle radius and density: the effect of evaporation

Let us justify that it is an acceptable physical assumption to consider $m_p(t) \neq 0, \forall t \in [0, T_e]$.

Following for example [4, 19] and [28], the evolution of $R(t)$ can be described, in a simplified form, by

$$R(t) = \begin{cases} R_0(1 - \frac{\theta(1-RH)t}{R_0^2})^{\frac{1}{2}}, & t \leq t_{ev}, \\ R_0(\frac{\phi_0}{1-RH})^{\frac{1}{3}}, & t > t_{ev}. \end{cases} \tag{7}$$

In (7) $R_0 > 0$ is the initial radius of the particles, θ is a physical parameter, RH represents relative humidity, ϕ_0 is the volume proportion of non-volatile content and t_{ev} is the evaporation time with $t_{ev} \ll T_e$. The parameter θ has a constant value, $\theta = 1.1 \times 10^{-}9 \quad m^2/s$ ([4]). Respiratory particles are liquid droplets that contain non-volatile nuclei, composed by sugars, proteins, lipids and pathogens. The typical volume proportion of the non-volatile content, ϕ_0, satisfies

$$1\% \leq \phi_0 \leq 10\%.$$

The previous arguments justify that $R(t)$ is a decreasing function of t but $R(t) \neq 0$, for every t and consequently that $m_p(t) \neq 0$ in $[0, T_e]$. The evaporation time, t_{ev}, is obtained from equations (7) by assuming continuity of $R(t)$, that is by equaling the values of $R(t_{ev})$ given by the two expression in (7).

As the radius $R(t)$ shrinks, the density of the particles, $\rho_p(t)$, increases because the nuclei are denser than the evaporating water (Fig. 2 and Fig. 5). Assuming that particles keep a spherical shape, while evaporating, we have

$$\rho_p(t) = \begin{cases} 1 + (\rho_p^n - 1)\frac{R_0^3\phi_0}{R^3(t)(1-RH)}, & t \leq t_{ev} \\ \rho_p^n, & t > t_{ev}, \end{cases} \tag{8}$$

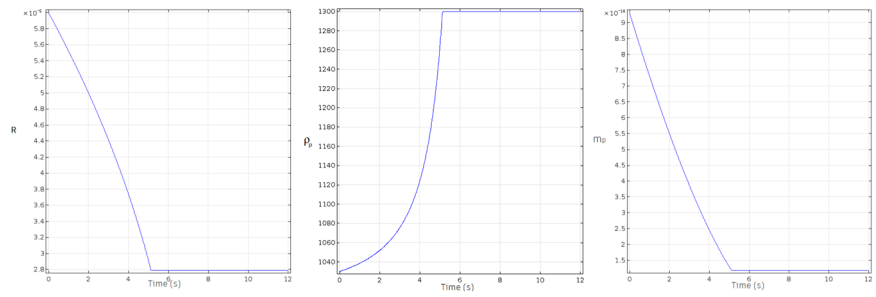

Figure 5 Plots of R, ρ_p and m_p during 12 seconds

where ρ_p^n is the density of the non-volatile nuclei, that is the final density of the particle. The expression for $\rho_p(t)$ for $t \leq t_{ev}$ is deduced from (8)

$$\rho_p(t) = \frac{(R^3(t) - R_0^3\phi_0^*) + R_0^3\phi_0^*\rho_p^n}{R^3(t)}, \tag{9}$$

where $\phi_0^* = \phi_0/(1-RH)$. Values for ρ_p^n depend on the nuclei composition and can be found in experimental studies. For example for Sars-Cov-2 a density of $1.3\,g/ml$ is suggested in the experimental study [24].

We illustrate the time behaviour of R, ρ_p and m_p in Fig. 5 for $R_0 = 60\ \mu m$ and $RH = 0.5$. It can be observed that R and m_p are time decreasing and ρ_p is an increasing function of time.

2.3 The drift flux model

In the present paper we use a drift flux model. Drift flux models have been addressed by several authors from a theoretical point of view or from an applied viewpoint. We mention without being exhaustive ([5, 8, 10, 12, 28]). The principles underlying this class of models are the following:

1. Conservation of momentum is established for the mixture: air and particles;
2. Conservation of mass is established for the two phases separately;
3. Relative motion of the particles, with respect to airflow, is essentially due to the gravitational settling of the dispersed phase.

The mixture momentum equation and the mass conservation are given by ([17])

$$\begin{cases} \rho_f \dfrac{\partial u_f}{\partial t} + \rho_f (u_f \cdot \nabla) u_f = \nabla \cdot (\mu_{eff} \nabla u_f) - \nabla p \\ \nabla \cdot (\rho_f u_f) = 0, \quad \text{in } \Omega \times (0, T_e], \end{cases} \tag{10}$$

where u_f is the air flow velocity, ρ_f stands for air density, μ_{eff} represents the effective diffusion and p represents the atmospheric pressure. We observe that a simplification is made when considering that ρ_f represents air density and not the mixture density. The approximation is justified by the small volume of respiratory particles when compared with the air volume in Ω. This simplification implies that ρ_f is assumed constant in time. Equation (10) describes the mixture and not the two phases, using a momentum and mass conservation for the airflow with the hypothesis $\rho_f = \rho$.

Following principle 3, of the drift flux models, the velocity field, that represents the velocity of particles travelling in the airflow, is defined as $u_f + u_s$, where u_f is given by equation (10) and u_s is the relative velocity of particles with respect to airflow. It is defined as the settling velocity, u_s ([28, 31]). The settling velocity u_s, which equation we will deduce in what follows, is given by the steady state solution of system (1).

From equation (6) and defining the flux $J = -D\nabla C + (u_f + u_s)C$, where D stands for the diffusion coefficient we can conclude that mass conservation of evaporating particles, with non-volatile nuclei is equivalent to a convection-diffusion-reaction equation for the density number of particles that reads

$$\frac{\partial C}{\partial t} + \nabla \cdot \big((u_f + u_s)C\big) = \nabla \cdot (D\nabla C) - (K + V)C \quad \text{in } \Omega \times (0, T_e]. \tag{11}$$

For high Reynolds number of the flow, Re, $D = D_B + \epsilon$, where D_B is the Brownian diffusion and ϵ is the eddy diffusivity ([28]).

To compute the settling velocity of the particle, u_s, let us now return to system (1). As F_s, the force responsible for the momentum destruction of vapour due to evaporation, is defined by $-\frac{dm_p}{dt}u_p$ ([6]), we have from (1)

$$m_p \frac{du_p}{dt} = F_g + F_b + F_d, \tag{12}$$

where the gravity force, F_g, the buoyancy, F_b, and the drag force, F_d, are defined respectively by

$$\begin{cases} F_g = \frac{4}{3}\pi R^3 g \rho_p, \\ F_b = -\frac{4}{3}\pi R^3 g \rho_f, \\ F_d = \frac{1}{2} C_d \rho_f \pi R^2 \|u_f - u_p\|(u_f - u_p). \end{cases} \tag{13}$$

In (13), $\|.\|$ denotes the $L^2(\Omega)$ norm (for scalar and vector functions) defined as $\|u\| = \left(\int_\Omega |u|^2\, dx\right)^{\frac{1}{2}}$, where $|u|^2 = u \cdot u$ denotes the Euclidean inner product; R and ρ_p are time functions that represent the particle's radius and density defined in (7) and (9) respectively. As the theoretical results presented in the present paper hold for two and three dimensions the gravitational acceleration is represented by $g = (0, -9.8)$ or $g = (0, 0, -9.8)$ respectively. C_d stands for the drag coefficient defined in [6] as

$$C_d = \frac{21.12}{Re_p} + \frac{6.3}{\sqrt{Re_p}} + 0.25. \tag{14}$$

The behavior of C_d as a function of Re_p is represented in Fig. 6, where Re_p stands for the Reynolds number of the particle.

Equation (14) represents an empirical relation that holds for particles with Reynolds number, Re_p, such that $0.2 < Re_p < 2 \times 10^3$. We define Re_p as in [25] by

$$Re_p = \frac{2\rho_f R \|u_f - u_p\|}{\upsilon}, \tag{15}$$

where υ is the kinematic viscosity of air and $n = 2, 3$. As Re_p is not constant, because radius and velocity are time dependent, we illustrate in Table 1, the maximum value of the particle

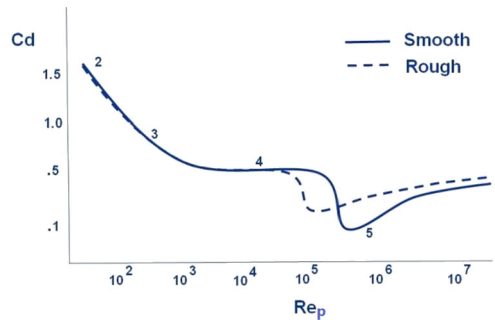

Figure 6 The behaviour of the drag coefficient C_d as a function of Re_p for smooth and rough spheres. Image retrieved August 31, 2023, from https://www1.grc.nasa.gov/beginners-guide-to-aeronautics/drag-of-a-sphere/

Table 1 Maximum value of particle's Reynolds number (Re_p)

R_0 (μm)	Max Re_p
2	2.688
60	80.6

Reynolds number for initial radii $R_0 = 1$ μm and $R_0 = 60$ μm. The values are computed from equation (15). We select these two values of R_0 as representative of expelled particles because around 95% of these particles have radii that stay in the interval $[1, 60]$.

The settling velocity, u_s, is the steady solution of (12), (13) under quiescent conditions, that is when $u_f = 0$ ([31]). As the settling velocity has the same direction as gravity - it points downward, perpendicularly - only its second or third component is not zero. We represent this component by $\bar{u}_s$. Assuming that the steady state is achieved for $t > t_{ev}$, we have from (7)

$$|\bar{u}_s| = \sqrt{\frac{8|g|R_0(\frac{\phi_0}{1-RH})^{\frac{1}{3}}(\rho_p^n - \rho_f)}{3C_d^*\rho_f}}. \tag{16}$$

In (16), $|g| = 9.8$ and C_d^* is the steady state value for the drag coefficient C_d given in (14). As the particle Reynolds number at the steady state is defined by

$$2\rho_f R_0\big(\phi_0/(1-RH)\big)^{1/3}|\bar{u}_s|/\nu,$$

the settling velocity can be calculated only iteratively from (15) and (16). For the purposes of the theoretical estimates presented in Sect. 3, we circumvent such difficulty, by using superior and inferior bounds for C_d^*, computed from the previous assumption that the particle Reynolds number satisfies $0.2 < Re_p < 2 \times 10^3$. In this case we have $C_d(0.2) < C_d^* < C_d(2 \times 10^3)$, where $C_d(\cdot)$ is the drag coefficient defined in (14).

2.4 Initial and boundary conditions

The boundary conditions of the model are defined by:

- for the velocity u_f (defined by (10))

$$\begin{cases} u_f \cdot \eta = -u_w & \text{on } \partial\Omega_W \times (0, T_e], \\ u_f \cdot \eta = -u_{f_{in}} & \text{on } \partial\Omega_{M_f} \times (0, T_e], \end{cases} \tag{17}$$

  where η stands for the exterior unitary normal to each boundary. A no-slip boundary condition for u_f, that is $u_f = 0$, is imposed on $(\partial\Omega \setminus (\partial\Omega_W \cup \partial\Omega_{M_f})) \times (0, T_e]$. In equation (17), u_w is related to a passive ventilation velocity coming from the windows and $u_{f_{in}}$ is associated to the velocity of the respiratory airflow.

  In the framework of the theoretical model no restrictions are made on u_w and $u_{f_{in}}$.
- for the number density of respiratory particles C

$$\begin{cases} J \cdot \eta = \alpha_W C & \text{on } \partial\Omega_W \times (0, T_e], \\ J \cdot \eta = \alpha_D C & \text{on} \partial\Omega_D \times (0, T_e], \\ J \cdot \eta = 0 & \text{on } \partial\Omega_F \times (0, T_e], \\ J \cdot \eta = 0 & \text{on } (\partial\Omega_{w_a} \cup \partial\Omega_{M_b}) \times (0, T_e], \\ J \cdot \eta = -\frac{E(t)}{|\partial\Omega_{M_f}|} & \text{on } \partial\Omega_{M_f} \times (0, t_d], \\ J \cdot \eta = 0 & \text{on } \partial\Omega_{M_f} \times (t_d, T_e], \end{cases} \tag{18}$$

  where $J = -D\nabla C + (u_f + u_s)C$, t_d is the duration of the respiratory event ($t_d < T_e$), $E(t)$ represents the number of particles emitted by time unit and $|\partial\Omega_{M_f}|$ stands for the measure of $\partial\Omega_{M_f}$. We observe that there are a number of techniques used to measure $E(t)$ as laser scattering particle spectrometers and aerodynamic particle sizers ([30]). The permeability constants α_W and α_D are positive, which means that the particles can fly outwards from the door and the window.

Null initial conditions are assumed for the velocity u_f, for the pressure and for the number density of particles C.

3 Qualitative behaviour

An energy estimate that proves the stability of the model for finite times is presented in this section. An expression for the total number of particles is also established. The upper bound of this expression depends on a number of parameters that characterize the driving factors (Fig. 1). The qualitative behaviour of this estimate leads to results in agreement with experimental literature.

We begin by establishing an energy estimate for the concentration C. We omit the space and time independent variables. Multiplying equation (11) by C and taking the integral in Ω we have

$$\frac{1}{2}\frac{d}{dt}\|C\|^2 + \int_\Omega \nabla \cdot \big((u_f + u_s)C\big)C\,dx = \int_\Omega \nabla \cdot (D\nabla C)C\,dx - S\|C\|^2, \tag{19}$$

where the sink S is defined by

$$S = K + V, \tag{20}$$

and $\|\cdot\|$ denotes the usual norm in $L^2(\Omega)$. In (20), we recall that V represents the inactivation rate of the pathogen and that K represents a global deposition rate, defined in ([1]) by

$$K = \frac{|\bar{u}_s|}{H}, \tag{21}$$

where $\bar{u}_s$ stands for the last component of the perpendicular settling velocity, given in (16), and H is the height of the emission source. From (16), (20) and (21) we deduce that S is defined by

$$S = S(RH, R_0) = \left[\frac{8}{3}\frac{R_0}{C_D^*}\left(\frac{\phi_0}{1-RH}\right)^{1/3}|g|\frac{\rho_p^n-\rho_f}{\rho_f}\right]^{\frac{1}{2}}\frac{1}{H} + V, \tag{22}$$

where the dependence of S on RH and R_0 is explicited.

As

$$\int_\Omega \nabla\cdot\big((u_f+u_s)C\big)C\,dx = -\int_\Omega (u_f+u_s)C\cdot\nabla C\,dx + \int_{\partial\Omega}(u_f+u_s)\cdot\eta C^2\,d\omega,$$

and

$$\int_\Omega \nabla\cdot(D\nabla C)C\,dx = -\int_\Omega D\|\nabla C\|^2\,dx + \int_{\partial\Omega} DC\nabla C\cdot\eta\,d\omega,$$

from (19) we have

$$\frac{1}{2}\frac{d}{dt}\|C\|^2 = -D\|\nabla C\|^2 + \int_\Omega (u_f+u_s)C\cdot\nabla C\,dx - \int_{\partial\Omega} CJ\cdot\eta\,dw - S\|C\|^2. \tag{23}$$

We note that u_s does not depend on t. Assuming that $u_f + u_s \in L^\infty(\Omega)$, we have from (23)

$$\begin{aligned}&\frac{d}{dt}\|C\|^2 + \big(2D-\beta^2\big)\|\nabla C\|^2 - h(t)\|C\|^2 + 2\sum_{i=W,D}\alpha_i\|C\|^2_{L^2(\partial\Omega_i)}\\ &\quad - 2\int_{\partial\Omega_{M_f}}\frac{E(t)}{|\partial\Omega_{M_f}|}C\,d\omega < 0, \quad t\in(0,T_e],\end{aligned} \tag{24}$$

where $\beta \neq 0$ is an arbitrary constant. In equation (24), $h(t) = \frac{\|u_f+u_s\|^2_{L^\infty(\Omega)}}{\beta^2} - 2S(RH,R_0)$ and $E(t) = 0$, $t > t_d$.

The last integral term in the first member of (24) satisfies

$$2\int_{\partial\Omega_{M_f}}\frac{E(t)}{|\partial\Omega_{M_f}|}C\,d\omega \le \frac{1}{\delta^2}\frac{1}{|\partial\Omega_{M_f}|}E^2(t) + \delta^2\|C\|^2_{L^2(\partial\Omega_{M_f})}, \tag{25}$$

where $\delta \neq 0$.

Replacing (25) in (24) we obtain

$$\begin{aligned}&\frac{d}{dt}\|C\|^2 + \big(2D-\beta^2-\delta^2\big)\|\nabla C\|^2 - \big(h(t)+\delta^2K_T\big)\|C\|^2\\ &\quad\le -2\sum_{i=W,D}\alpha_i\|C\|^2_{L^2(\partial\Omega_i)} + \frac{1}{\delta^2}\frac{1}{|\partial\Omega_{M_f}|}E^2(t),\end{aligned} \tag{26}$$

where K_T is a constant resulting from the application of a Trace Theorem ([7]) to $\|C\|^2_{L^2(\partial\Omega_{M_f})}$. Selecting β and δ such that $2D - \beta^2 - \delta^2 K_T > 0$ we establish

$$\|C\|^2 \leq \int_0^t e^{\int_s^t (h(\mu)+\delta^2 K_T)\,d\mu} \frac{1}{\delta^2} \frac{1}{|\partial\Omega_{M_f}|} E^2(s)\,ds, \quad t \in [0, T_e], \tag{27}$$

and using the definition of $h(t)$ we finally have

$$\|C\|^2 \leq \int_0^t e^{-2S(RH,R_0)(t-s)} e^{\int_s^t (\frac{\|u_f(\mu)+u_s\|^2_{L^\infty(\Omega)}}{\beta^2}+\delta^2 K_T)\,d\mu} \frac{1}{\delta^2} \frac{1}{|\partial\Omega_{M_f}|} E^2(s)\,ds. \tag{28}$$

Inequality (28) proves the stability, for fixed time T_e, of the initial boundary value problem defined by equation (11) with the boundary conditions (18).

Let us now estimate the total number of respiratory particles in the room.

The total number of respiratory particles suspended in the air, N, with initial radius R_0, is represented by $\int_\Omega C\,dx$. Integrating the two members of equation (11) in Ω, we have

$$\frac{dN}{dt}(t) = \int_{\partial\Omega} -J \cdot \eta\,d\omega - S(RH, R_0)N(t). \tag{29}$$

Computing then a solution of (29) we have

$$N(t) = \int_0^t e^{-S(RH,R_0)(t-s)} \left[E(s) - \sum_{i=W,D} \alpha_i \int_{\partial\Omega_i} C(s)\,d\omega \right] ds. \tag{30}$$

As $\alpha_i \geq 0$, $i = W, D$, from (30) we conclude

$$N(t) \leq \int_0^t e^{-S(RH,R_0)(t-s)} E(s)\,ds, \tag{31}$$

assuming that the concentration C is positive. In (31) C_d^* is replaced by $C_{d,\max}$ in the definition (22) of $S(RH, R_0)$.

From the previous results we can establish the conclusions that follow.

1. $N(t)$ is a decreasing function of the initial radius of the particle, R_0. The conclusion has a sound physical meaning because large droplets deposit first and consequently remain suspended in the air for less time ([6]). The plots in Figs. 8, 9 and 10 computed numerically, as detailed in Sect. 4, illustrate the theoretical result.
2. $N(t)$ is a decreasing function of RH, the relative humidity. The higher the relative humidity, the lower the evaporation rate. Therefore under the action of high humidity particles fall first to the floor, and consequently remain suspended in the air for less time ([4]). This result is illustrated in the plot of Fig. 10, computed numerically from the model.
3. The total number of particles $N(t)$ increases with $\hat{E}$, defined as the total number of particles emitted during the event. The numerical result in Fig. 12 illustrates why large emissions characterize super-spreader's events.
4. The increase of $N(t)$ with the rate of exhalation, defined in (17), can be established from (28). However, for the parameters used in the numerical simulations, the influence of $u_{f_{in}}$ is not meaningful (Fig. 13).

Table 2 Variables and parameters used in the simulations

Variable/Parameter	Value	Unit	Description
m_p		g	mass of a particle
C		n/m^3	number density of particles
K		1/s	deposition rate
V	0.01, 0.028	1/s	inactivation rate ([1])
J		n/(m^{2}s)	convection diffusion flux
R_0	2, 60	μm	initial radius ([27])
ϕ_0	0.1	-	percent of non volatile content ([4])
RH	0.5, 0.8	-	relative humidity ([1])
t_{ev}	5	s	evaporation time
t_d	0.5	s	duration of the respiratory event
T_e	10	s	observation time
ρ_p^n	998.6	Kg/m^3	nucleus density ([6])
D	1.8×10^{-5}	m^2/s	diffusion coefficient ([23])
ρ_f	1.2077	Kg/m^3	fluid density ([6])
μ	1.8×10^{-5}	m^2/s	effective viscosity ([23])
p		Pa	atmospheric pressure
$\|g\|$	9.8	m/s^2	gravity acceleration
C_d			drag coefficient
u_s		m/s	settling velocity of the particles
$u_{f_{in}}$		m/s	inlet velocity profile ([11]) - cough event
u_w	0.1, 2	m/s	last component of an horizontal ventilation velocity
α_W, α_D	1	m/s	transfer coefficient - particle's flux

4 Numerical illustrations

The theoretical results of Sect. 3 have been established in $\mathbb{R}^n$, $n = 2, 3$. In Sect. 4 we illustrate numerically these results for $n = 2$. We also exhibit plots illustrating the behaviour of $N(t)$ with $u_{f_{in}}$ and u_w (equation (17)). The problem is solved in the two-dimensional geometry Ω, with 4 m wide and 2.5 m high, represented in Fig. 3 using Comsol Multiphysics software (version 5.1), using the laminar flow and the transport of diluted species modules. A quadratic piecewise finite element for the concentration equation and a piecewise linear finite element for the velocity are considered. A triangular mesh automatically generated with 40,957 elements is used to obtain a consistent mesh. In the region of the inlet velocity profile for a cough event, $\partial\Omega_{M_f}$, the mesh is highly refined. We note that for the conditions considered in the numerical simulations presented in this section, the Reynolds number of the airflow does not exceed 2600. The time integration is performed with a backward difference method, with variable order ranging between 1 and 2 and an adaptative time step. The system of algebraic equations generated from the matrix assembly is solved using an affine invariant form of the damped Newton method. To compute the numerical solutions of the Navier-Stokes equation and of the concentration equation, (10) and (11), streamline diffusion and crosswind diffusion stabilizers were used in both equations.

The values used for the parameters in the numerical simulations are presented in Table 2.

Convergence tests have been carried out with meshes of decreasing size to verify that the solution is mesh independent. In Table 3 we present the relative errors for the concentrations considering a reference solution obtained with a mesh composed of 51,997 elements in Ω. We observe that an increase in the number of elements leads to a decreasing of the relative error. An increase of 3.75 times of the number of elements leads to a decrease in the relative error of 68 times at $t = 5$, of 132 times at $t = 7$ and of 325 times at $t = 10$.

Table 3 Relative error for the concentration with respect to the maximum norm at t = 5, 7 and 10

Number of elements	$t = 5$	$t = 7$	$t = 10$
10,931	0.34	0.66	1.30
22,417	0.13	0.25	0.46
30,799	0.127	0.22	0.37
40,957	0.005	0.005	0.004

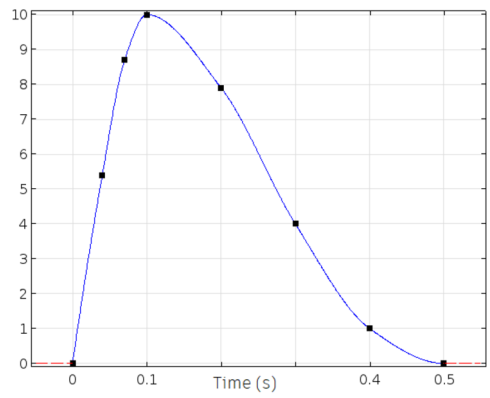

Figure 7 Inlet velocity profile $u_{f_{in}}$, for a cough event, defined on the boundary of $\partial\Omega_{M_f}$ (adapted from [11])

The problem is solved for small and large particles with two initial representative radius of 2 and 60 μm, respectively. To simulate a respiratory event of cough, the velocity profile $u_{f_{in}}$ presented in Fig. 7 is considered ([11]). The maximum velocity considered is 10 m/s and the event lasts for 0.5 seconds.

In order to study the differences between the paths of large and small particles, we exhibit in Fig. 8 the space-time evolution of particle distribution C for $R_0 = 2, 60$ μm at $t = 0.5, 1, 3$. A slight ventilation rate is considered (0.1 m/s) and relative humidity RH is fixed at 0.5. We note that, as expected, deposition is more significant for large particles. In addition large particles hit the floor up to 0.5 m; instead small particles remain essentially suspended in the air. In fact we observe that, at $t = 3$, large particles were deposited up to a distance of about 1 m from the horizontal projection of the emitter. Small particles behave differently. At $t = 3$ all particles remain suspended in the air and there is no visible deposition on the floor. At a distance of 2.5 a child can breathe in infected particles. These simulations suggest that for large particles the guidelines for a two meters social distancing, adopted by the World Health Organization, during Sars-Cov-2 pandemic, prevents the spread of disease. However, for small particles this social distancing is not enough.

To get a clearer view of the dependence of $N(t)$ on R_0, when a slight horizontal ventilation rate is considered (0.1 m/s), we exhibit in Fig. 9 the dependence of the total number of particles $N(t)$, on the initial radius R_0, during 10 seconds. More precisely the number of large particles ($R_0 = 60$) falls abruptly from $t = 2$, the number of small particles ($R_0 = 2$) remains constant during the observation period, $[0, 10]$.

We note that $N(t)$ is a decreasing function of R_0: large particles deposit first and have a smaller contribution to airborne dissemination. This conclusion can be established from Sect. 3.

To better understand the evolution of small particles in the room over time, the problem is solved under the same conditions as the results presented in Figs. 8 and 9 but for

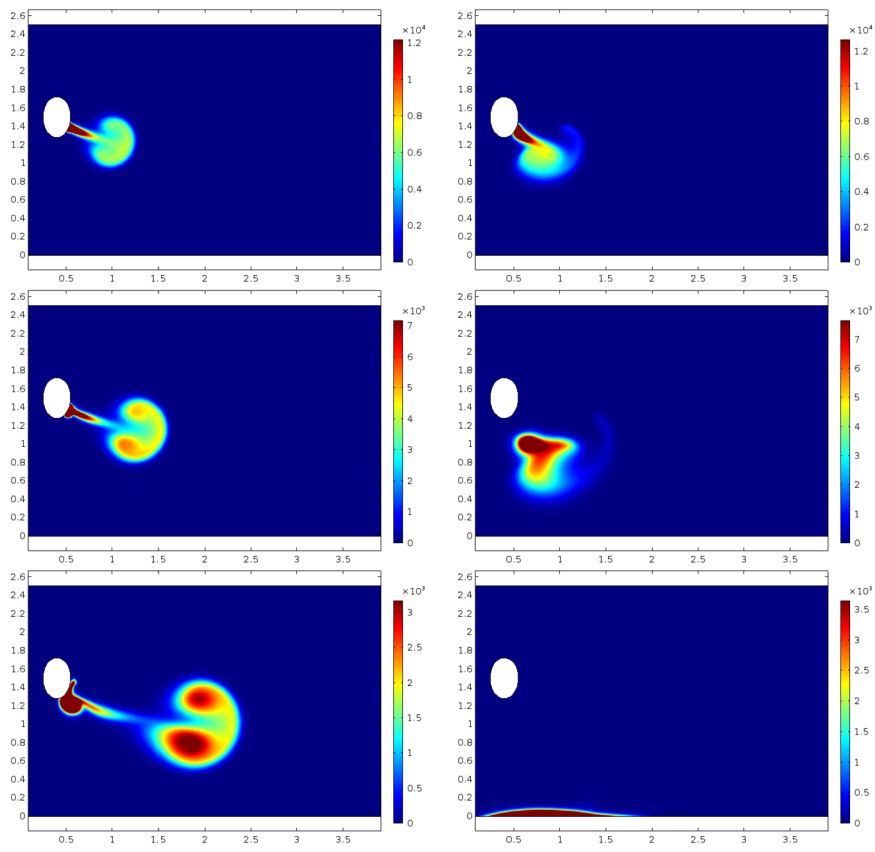

Figure 8 Concentration distribution C at $t = 0.5, 1, 3$ s: small particles $R_0 = 2$ - left, large particles $R_0 = 60$ - right ($u_w = 0.1$, $RH = 0.5$)

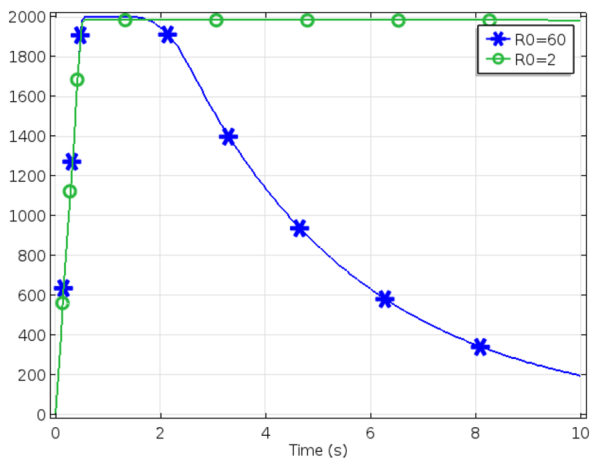

Figure 9 The dependence of $N(t)$ on R_0 during 10 seconds with $RH = 0.5$ and $u_w = 0.1$

a larger time, T_e = 20. The result is presented in Fig. 10. The number of small particles decreases after 10 seconds, instead of 2 seconds, for large particles. We observe that after 20 s, there are about 45% of small particles and practically no large particles. The result is

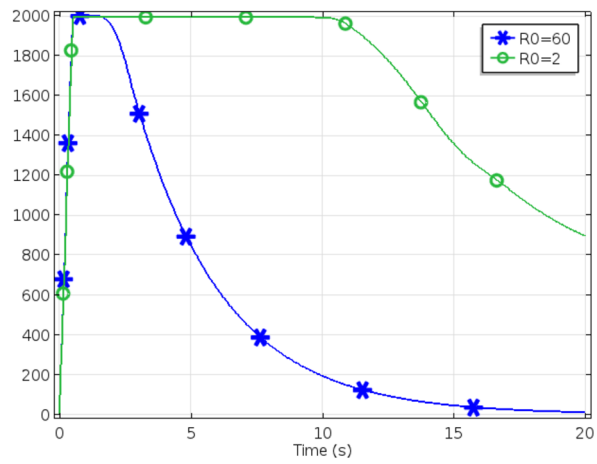

Figure 10 Behavior of the number of small and large particles ($R_0 = 2$, $R = 60$), during 20 seconds with $RH = 0.5$ and $u_w = 0.1$

physically sound because large respiratory particles fall to the ground more quickly than small particles.

The plots in Figs. 8, 9 and 10, computed from the numerical solution of the model, illustrate the theoretical results deduced from estimate (31), related to the behaviour of $N(t)$ with R_0. The reference values considered for the fixed parameters are $R0 = 60$, $u_w = 0.1$, $RH = 0.5$ and $E(t) = 4000$, where $E(t)$ stands for a constant number of emitted particles per unit time. The global number of particles emitted, $\hat{E}$, during an event that lasts $t_d = 0.5$, is 2000 as represented in the plots. We note that there are several techniques to measure the number of particles, of different radius, emitted during respiratory events, but its description falls outside the scope of the present paper.

In what follows the dependence of $N(t)$ on the relative humidity RH, the total emission of particles, $\hat{E}$, and the velocity of an horizontal room passive ventilation $(0, u_w)$ are illustrated.

In Fig. 11 the influence of relative humidity for small ($R_0 = 2$) and large particles ($R_0 = 60$) is illustrated without ventilation. We observe that an increase in the relative humidity implies a decrease in the number of suspended particles in the room. The difference is meaningful for heavy particles (at t = 4 the increase in RH from 0.5 to 0.8 implies a 20% decrease in $N(t)$ - there are 1000 particles for $RH = 0.5$ and about 800 particles for $RH = 0.8$), for small particles the influence of RH obeys the same principle but is not so significant.

The effect on $N(t)$ of the total number of particles emitted is plotted in Fig. 12 during 10 seconds, for $E(t) = 4000$, $E(t) = 8000$ and $t_d = 0.5$. A slight horizontal ventilation rate ($u_w = 0.1$ m/s) and $RH = 0.5$ are considered. As expected, the larger the emitting source, the greater the number of particles in the room.

In some indoors respiratory events a single infected person, called a super-spreader, is more likely to infect other people. Different reasons are invoked to explain these super-spreader events. We begin by mentioning biological reasons as a greater number of expelled particles, $\hat{E}$, and higher rates of emission $E(t)$ ([2]). The theoretical results in Sect. 3, illustrated by Fig. 12, confirm this hypothesis.

In Fig. 13 it is illustrated the influence of $u_{f_{in}}$, defined on the boundary of $\partial\Omega_{M_f}$ such that $u_f \cdot \eta = -u_{f_{in}}$. An increase in the expiration rate leads to a very slight increase of $N(t)$

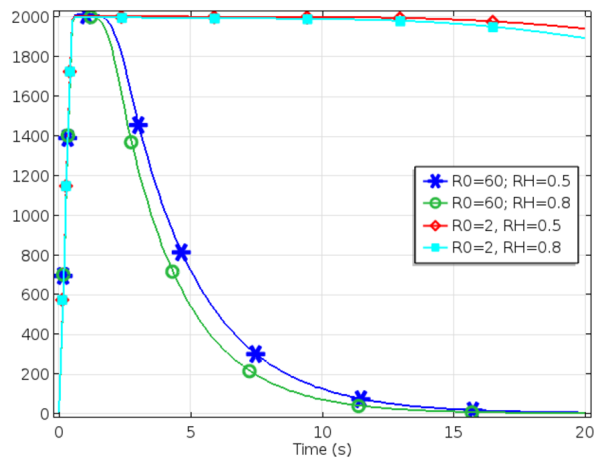

Figure 11 Influence of RH on $N(t)$ for small ($R_0 = 2$) and large ($R_0 = 60$) particles during 20 seconds, without ventilation

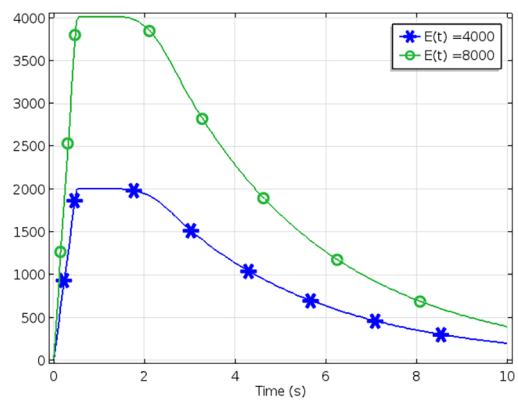

Figure 12 Influence of the total number of particles emitted, on $N(t)$ during 10 seconds ($R_0 = 60$, $RH = 0.5$, $t_d = 0.5$, $u_w = 0.1$)

during the two first seconds. We observe that the expiration velocity acts only during the duration of the event, $t_d = 0.5$, what can explain the very slight influence.

Another common feature of indoor super-spreader events is poor ventilation ([26]). The dependence of $N(t)$ on the ventilation, for small and large particles, is illustrated in Fig. 14 for $u_w = 0.1$, 2 over 10 seconds, for $R_0 = 2$ on the left and $R_0 = 60$ on the right ($RH = 0.5$). Ventilation keeps small particles suspended, preventing them from deposition; the larger is u_w the longer they stay suspended. After an initial period, the particles arrive at the door and leave the room. As particles transported by an horizontal ventilation with $u_w = 2$ arrive first than in a quiescent air, this can explain why after 10 seconds, in a well ventilated room, there are no more particles. Regarding large particles, deposition is dominant; consequently as it does not depend on u_w, the difference is less significant. The plots in Fig. 14 confirm the recommendations by health authorities, for an efficient natural ventilation. The dependence of $N(t)$ on ventilation is not deduced from the theoretical estimates.

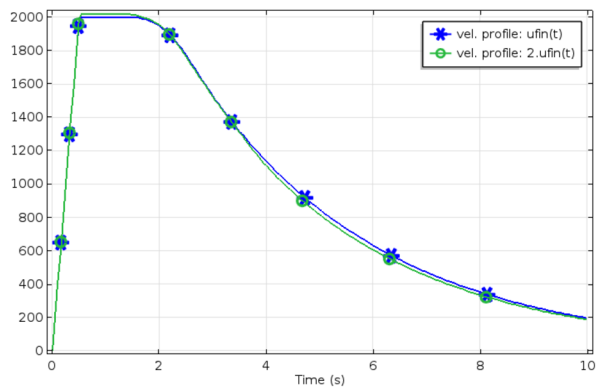

Figure 13 The influence of the inlet velocity on $N(t)$ ($R_0 = 60$, $RH = 0.5$, $t_d = 0.5$, $u_w = 0.1$)

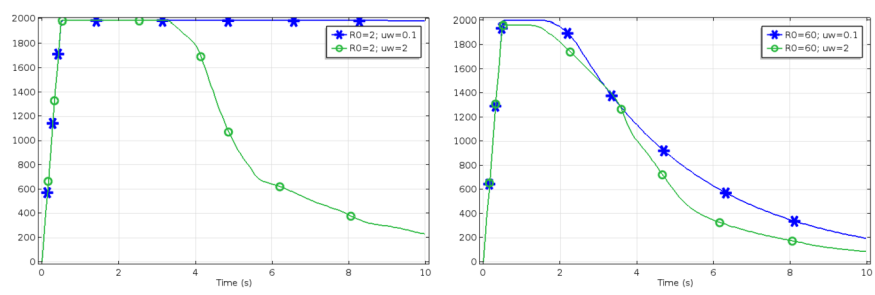

Figure 14 The effect of ventilation ($u_w = 0.1, 2$) on $N(t)$ over 10 seconds ($R_0 = 2$ on the left; $R_0 = 60$ on the right)

5 Final remarks

Inhaling indoor air is the primary mean by which people is exposed to respiratory particles. Knowledge of the trajectory of respiratory particles is essential to support the definition of guidelines that minimize airborne transmission of diseases. The study of the trajectory of respiratory particles is complex because it depends on a large number of phenomena and factors. As with all mathematical models, it is important to keep the description of phenomena as simple as possible, but exhibiting the main properties established by physical laws. Based on experimental studies we focus on a limited number of factors, related to intrinsic particle properties (the total number of particles emitted, the number of particles emitted by time unit, the initial radius, the expelling velocity) and to environmental properties (relative humidity).

We summarize in what follows the main conclusions established from the estimates, regarding the total number of airborne particles:

- The total number of airborne particles is a decreasing function of the initial radius R_0. The conclusion, established from the theoretical estimate (31), has a sound physical meaning because large droplets deposit first and consequently remain suspended in the air for less time ([3, 6]). Moreover, the plots in Figs. 8, 9 and 10, computed from the numerical solution of the model, illustrate the result. We observe that the plots in Fig. 8 suggest that, in the conditions of our simulations, for large particles the two meters social distancing, adopted by the World Health Organization, during Sars-Cov-2 pandemic, prevents the spread of disease for large particles. On the

contrary the plots in Fig. 8 (left) suggest that for small particles this social distancing is not enough. These last observations concerning social distance cannot be established from the theoretical estimates.

- The total number of airborne particles decreases with RH. This conclusion is in agreement with a number of experimental studies ([4, 20]) and suggests an explanation for the seasonality of respiratory infections. The rationale under this explanation is that in winter people spends more time indoor, with warmer temperatures, that dry the air coming from outdoors, which leads to a drop in RH. This causes a large evaporation rate and consequently a higher number of suspended respiratory particles. The numerical plots in Fig. 11 illustrate the influence of RH and suggests that its influence is more significant for large particles.
- The total number of airborne particles increases with the number of particles emitted per time unit, $E(t)$, and with the total number of particles emitted, $\hat{E}$. This conclusion is in agreement with the hypothesis of some researchers, that a small percent of people are responsible for a large number of infections ([14]). In fact researchers believe that, among other biological causes, this could be a consequence of individuals - the superspreaders - that emit a higher number of particles per time unit. The plots in Fig. 12 illustrate this influence.

Equation (31) does not allow us to draw conclusions about the behavior of $N(t)$ with ventilation. However the plot in Fig. 14, computed numerically from the model, confirm, in the conditions of the simulations, the recommendations of health authorities regarding ventilation. As mentioned in Sect. 1 future developments of the mathematical model should include the direct influence of temperature on the inactivation rate of virus ([29]).

Despite its simplicity, the model allows establishing a number of results in accordance with mounting epidemiological evidences and research work produced by different groups (for example [3, 21] and [22]).

Acknowledgements
The authors thank the anonymous referees for their helpful comments that improved the quality of the paper.

Funding
This work was partially supported by the Centre for Mathematics of the University of Coimbra- UIDB/00324/2020, funded by the Portuguese Government through FCT/MCTES, Fundação para a Ciência e Tecnologia (FCT)/Ministério da Ciência e Ensino Superior (MCTES)-(Portuguese Science Foundation/Ministry of Science and Higher Education).

Availability of data and materials
The values of the parameters used in the numerical simulations are included in the paper.

Declarations

Ethics approval and consent to participate
Ethics approval and consent to participate Not applicable.

Consent for publication
Consent for publication Not applicable.

Competing interests
The authors declare no competing interests.

Author contributions
All authors contributed to the paper equally, elaborating the model, making the theoretical study and performing the numerical simulations. All authors participated in the draft of the manuscript, read and approved its final form.

Authors' information
Email adresses J.A. Ferreira: ferreira@mat.uc.pt; Paula de Oliveira: poliveir@mat.uc.pt; P.M. da Silva: pascals@isec.pt.

Author details
[1]Centre of Mathematics of the University of Coimbra, University of Coimbra, FCTUC, 3030 Coimbra, Portugal.
[2]Polytechnic of Coimbra, ISEC, DFM, Rua Pedro Nunes, 3030-199 Coimbra, Portugal.

Received: 24 April 2023 Accepted: 16 November 2023 Published online: 12 January 2024

References

1. Aganovic A, Bib Y, Cao G, Drangsholt F, Kurnitski J, Wargocki P. Estimating the impact of indoor relative humidity on SARS-CoV-2 airborne transmission risk using a new modification of the Wells-Riley model. Build Environ. 2021;205:108–278.
2. Asadi S, Wexler AS, Cappa CD, Barreda S, Bouvier NM, Ristenpart WD. Aerosol emission and superemission during human speech increase with voice loudness. Sci Rep. 2019;9(2348):1–10.
3. Bourouiba L, Dehandschoewercker E, Bush JWM. Violent expiratory events: on coughing and sneezing. J Fluid Mech. 2014;745:537–63.
4. Bozic A, Kanduc M. Relative humidity in droplet and airborne transmission of disease. J Biol Phys. 2021;47:1–29.
5. Chen F, Simon CM, Lai ACK. Modeling particle distribution and deposition in indoor environments with a new drift flux model. Atmos Environ. 2006;40:357–67.
6. Cheng CH, Chow CL, Chow WK. Trajectories of large respiratory droplets in indoor environment: a simplified approach. Build Environ. 2020;183(107196):1–11.
7. Evans L. Partial differential equations. 2nd ed. Providence: Am. Math. Soc.; 2010.
8. Evje S, Flåtten T. On the wave structure of two-phase flow models. SIAM J Appl Math. 2007;67:487–511.
9. Flagan RC, Seinfeld JH. Fundamentals of air pollution engineering. New York: Prentice Hall; 1988.
10. Grossberg S, Jarman DS, Tabor GR. Derivation of the adjoint drift flux equations for multiphase flow. Fluids. 2020;5:31.
11. Gupta JK, Lin CH, Chen Q. Flow dynamics and characterization of a cough. Indoor Air. 2009;19:517–25.
12. Hibiki T, Ishii M. Distribution parameter and drift velocity of drift flux model in bubbly flow. Int J Heat Mass Transf. 2002;45:707–21.
13. Holmberg S, Li Y. Modelling of the indoor environment-particle dispersion and deposition. Indoor Air. 1998;8:113–22.
14. Illingworth CJR, Hamilton WL, Warne B, Routledge M, Popay A, Jackson C, Fieldman T, Meredith LW, Houldcroft CJ, Hosmillo M, Jahun AS, Caller LG, Caddy SL, Yakovleva A, Hall G, Khokhar FA, Feltwell T, Pinckert ML, Georgana I, Chaudhry Y, Curran MD, Parmar S, Sparkes D, Rivett L, Jones NK, Sridhar S, Forrest S, Dymond T, Grainger K, Workman C, Ferris M, Gkrania-Klotsas E, Brown NM, Weekes MP, Baker S, Peacock SJ, Goodfellow IG, Goulliouris T, Angelis D, Török ME. Superspreaders drive the largest outbreaks of hospital onset COVID-19 infections. eLife. 2021;10:e67308.
15. Katre P, Banerjee S, Balusamy S, Sahu KC. Fluid dynamics of respiratory droplets in the context of COVID-19: airborne and surface borne transmissions. Phys Fluids. 2021;33(081302):11–9.
16. Kumar S, Lee HP. The perspective of fluid flow behavior of respiratory droplets and aerosols through the facemasks in context of SARS-CoV-2. Phys Fluids. 2020;32:1–15.
17. Ladyzhenskaya OA. The mathematical theory of viscous incompressible flow. 2nd ed. New York: Gordon and Breach; 1969.
18. Morris DH, Yinda KC, Gamble A, Rossine FW, Huang Q, Bushmaker T, Fischer RJ, Matson MJ, Doremalen NV, Vikesland PJ, Marr LC, Munster VJ, Lloyd-Smith JO. Mechanistic theory predicts the effects of temperature and humidity on inactivation of SARS-CoV-2 and other enveloped viruses. eLife. 2021;10:e65902.
19. Netz RR. Mechanisms of airborne infection via evaporating and sedimenting droplets produced by speaking. J Phys Chem B. 2020;124:7093–101.
20. Paynter S. Humidity and respiratory virus transmission in tropical and temperate settings. Epidemiol Infect. 2015;143:1110–8.
21. Pendara MR, Páscoa JC. Numerical modeling of the distribution of virus carrying saliva droplets during sneeze and cough. Phys Fluids. 2020;32:1–18.
22. Quiñones JJ, Doosttalab A, Sokolowski S, Voyles RM, Castñano V, Zhang LT, Castillo L. Prediction of respiratory droplets evolution for safer academic facilities planning amid COVID-19 and future pandemics: a numerical approach. J Build Eng. 2022;54:104593.
23. Rosti ME, Cavaiola M, Olivieri S, Seminara A, Mazzino A. Turbulence role in the fate of virus-containing droplets in violent expiratory events. Phys Rev Res. 2021;3(013091):1–10.
24. Stadnytskyi V, Bax CE, Bax A, Anfinrud P. The airborne lifetime of small speech droplets and their potential importance in SARS-CoV-2 transmission. Biol Sci. 2020;117:11875–7.
25. Wang H, Li Z, Zhang X, Zhu L, Liu Y, Wang S. The motion of respiratory droplets produced by coughing. Phys Fluids. 2020;32(125102):1–14.
26. Wessendorf L, Richter E, Schulte B, Schmithausen RM, Exner M, Lehmann N, Coenen M, Fuhrmann C, Kellings A, Husing A, Jockel KH, Streeck H. Dynamics, outcomes and prerequisites of the first SARS-CoV-2 superspreading event in Germany in February 2020: a cross-sectional epidemiological study. BMJ J Open. 2022;12(4):e059809.
27. Xie X, Li Y, Sun H, Liu L. Exhaled droplets due to talking and coughing. J R Soc. 2009;6:S703–14.
28. Yang Y, Chan WY, Wu CL, Kong RYC, Lai ACK. Minimizing the exposure of airborne pathogens by upper-room ultraviolet germicidal irradiation: an experimental and numerical study. J R Soc Interface. 2012;9:3184–95.
29. Yap TF, Liu Z, Shveda RA, Prestona DJ. A predictive model of the temperature-dependent inactivation of coronaviruses. Appl Phys Lett. 2020;117:060601.
30. Zhang J, Zhang Z, Hou L, Zhou W. A novel optical instrument for measuring mass concentration and particle size in real time. Sensors. 2023;23:3616.
31. Zhao B, Zhan Z, Li X. Numerical study of the transport of droplets or particles generated by respiratory system indoors. Build Environ. 2005;40:1032–9.

Publisher's Note